DEUTSCHES ELEKTRONEN-SYNCHROTRON DESY

DESY 88-020
February 1988

CHARACTERISTICS OF HEAVY FLAVOUR PRODUCTION IN ep COLLISIONS

by

G. Ingelman, G. A. Schuler

Deutsches Elektronen-Synchrotron DESY, Hamburg

ISSN 0418-9833

NOTKESTRASSE 85 · 2 HAMBURG 52

To be sure that your preprints are promptly included in the
HIGH ENERGY PHYSICS INDEX ,
send them to the following address (if possible by air mail) :

DESY
Bibliothek
Notkestrasse 85
2 Hamburg 52
Germany

DESY 88-020
February 1988

ISSN 0418-9833

Characteristics of Heavy Flavour Production in *ep* Collisions

G. Ingelman, G.A. Schuler
Deutsches Elektronen-Synchrotron DESY
Notkestrasse 85, D-2000 Hamburg 52, FRG

Abstract

The production of heavy flavours in *ep* collisions at the HERA energy is studied using a model based on boson-gluon fusion into a heavy quark-antiquark pair followed by gluon emission and string hadronization. Total cross-sections and dependence on basic kinematical variables are given as well as distributions of the most important variables at both the quark and hadron level, e.g. rapidity and transverse momentum. Charm, bottom and top production is compared and signatures for their separation are discussed in terms of decay muons and global event shape properties.

1 Introduction

The physics of heavy quark flavours has several interesting aspects. Firstly, there are well-defined production processes that can be calculated in perturbative QCD at the quark level. Secondly, the fragmentation into hadrons is rather different from that of light quarks. Thirdly, the heavy flavour hadron states and their decays show a rich structure with interesting phenomena, e.g. different life times and $B^0 - \bar{B}^0$ mixing. The purpose of this paper is to study the basic phenomenology of heavy quark production in high energy *ep* collisions, such as will take place at HERA in a few years, in order to indicate the feasibility of experimental investigations of these issues.

The dominating production arises through the boson-gluon fusion into a heavy quark-antiquark pair. The cross-sections are expected to be large [1]. In fact, huge for charm and big enough for bottom to make HERA a $b\bar{b}$ 'factory'. The cross-section for top quark production should be large enough for experimental observation as long as the top quark mass does not exceed ~ 85 GeV. Indeed there is a window of opportunity for HERA to actually discover the top quark, namely if its mass is in the range 55–85 GeV. Of course, the usefullness of these cross-sections depends on the experimental possibility to actually observe and measure these events. This possibility in turn depends on the characteristic event features in terms of distribution in phase space, event shape properties and, e.g., the typical rapidity and transverse momentum of the heavy mesons and their decay muons. These issues are examined in the present paper with a positive result indicating that investigations of various QCD effects, extraction of the gluon structure function etc. could be within reach and should be examined in greater detail.

In order to make a detailed study we have constructed a Monte Carlo simulation model [2] based on the following main ingredients: *(i)* The complete matrix elements to order $\alpha^2\alpha_s$ for the boson-gluon fusion process [1] (including the masses of the produced heavy quarks and the full electroweak structure of the interaction), *(ii)* gluon emission from the $Q\bar{Q}'$ system in a parton cascade approach [3] and *(iii)* hadronization with the Lund string model [4] and heavy flavour decay. In Section 2 we specify the model, give results on total cross-sections and discuss the uncertainties of the calculation. The essential distributions with respect to event kinematics and the $Q\bar{Q}'$ pair as a whole are given in Section 3. More detailed properties of the produced heavy quarks and hadrons are presented in Section 4. A first study of heavy flavour signatures in terms of decay muons and event shape measures is performed in Section 5 and we end with a short discussion in Section 6.

2 Basic Processes and Cross-sections

In the leading order quark-parton model (QPM) heavy quark production occurs through mixing in the charged current (CC) process

$$e + q \rightarrow \nu + Q \tag{1}$$

as shown in Fig. 1a. The cross-section can be estimated by simply multiplying the deep inelastic scattering (DIS) cross-section with the appropriate Cabibbo-Kobayashi-Maskawa matrix element, $V^2_{ff'}$, between quark flavours f and f', giving

$$\sigma(Q) = \sum_f V^2_{Qf}\,\sigma_f \tag{2}$$

Here σ_f is the total ep cross section for interaction with a quark of flavour f in the proton. Due to the tiny mixing angles between the light quarks in the proton and the heavy quarks one expects very small cross-sections for this mechanism. For our numerical results below we have taken the heavy quark threshold approximately into account by requiring a sufficiently large mass of the final hadron system, $W > (m_Q + m_p)$. The condition $Q^2 > 1$ GeV^2 is also imposed in order to use the QPM cross-section formalism.

With heavy quark components in the proton larger mixing angles will appear and also neutral current (NC) processes become relevant, but the production is on the other hand suppressed due to the smallness of such heavy quark structure function parametrisations [5]. Furthermore, these are only effective approximations of higher order processes and should, in particular, not be used for calculations close to threshold.

The next-to-leading order process giving heavy quarks is the boson-gluon fusion (BGF) mechanism

$$V(q) + g(p) \rightarrow Q_f(p_f) + \bar{Q}_{f'}(p_{f'}) \tag{3}$$

occuring as $\mathcal{O}(\alpha_s\alpha^2)$ parton level subprocess in the ep scattering process (Fig. 1b)

$$e^{\pm}(l_e) + p(P) \rightarrow l'(l') + Q_f(p_f) + \bar{Q}_{f'}(p_{f'}) + X \tag{4}$$

Here the symbols in brackets denote the corresponding 4-momenta. In the CC case V is the $W^{\pm}$-boson whereas in the NC case it corresponds to γ/Z^0 exchange and the produced quark and antiquark have the same flavour f. The gluon, entering the subprocess eq. (3), carries a fraction x_g of the proton momentum, i.e. $p = x_g P$. As usual, we take $\hat{s}$ to denote the invariant mass square of the $Q\bar{Q}'$-subsystem, i.e. $\hat{s} = (p_f + p_{f'})^2$.

Beside the normal DIS variables defined by

$$\begin{aligned} Q^2 &\equiv -q^2 = -(l_e - l')^2 \\ W^2 &\equiv (P+q)^2 \\ x &\equiv \frac{Q^2}{2P\cdot q} \\ y &\equiv \frac{P\cdot q}{P\cdot l_e} \end{aligned} \tag{5}$$

out of which only two are independent, we need three additional independent variables to completely specify the process in eq. (4). For these we have chosen the gluon momentum fraction x_g, the variable

$$z = \frac{P\cdot p_f}{P\cdot q} \tag{6}$$

and the azimuthal (around the boson axis) angle Φ between the lepton and hadron planes

$$\cos\Phi = \frac{(\vec{p}\times\vec{l_e})\cdot(\vec{p}\times\vec{p_f})}{|\,\vec{p}\times\vec{l_e}\,||\,\vec{p}\times\vec{p_f}\,|} \tag{7}$$

measured in the boson-gluon CM frame, i.e. $\vec{p}_f + \vec{p}_{f'} = 0$. The variable z is related to the angle of the $Q\bar{Q}'$-axis with respect to the boson-gluon axis in this subsystem cms and gives the heavy quark transverse momentum through the relation $p_\perp^2 = \hat{s}z(1-z)+z(m_{f'}^2-m_f^2)-m_f^2$. (Since Q^2 is dominantly close to zero, see below, there is usually no strong transverse boost to the laboratory frame and hence this also approximates the transverse momentum in the laboratory frame.)

The cross section for process (4) is then given by

$$\sigma(e^\pm p \to Q\bar{Q}'X) = \int dy \int dQ^2 \int dx_g \int dz \int d\Phi\; g(x_g, M_g^2)\, h(y, Q^2, x_g, z, \Phi) \tag{8}$$

which is a convolution of the gluon density $g(x_g, M_g^2)$ and a QCD part h for the subprocess. The latter has been calculated in ref. [1] taking proper account of the heavy quark masses and the complete electroweak structure for both charged and neutral current processes including the $\gamma - Z^0$ interference and allowing for arbitrary longitudinally polarization of the $e^\pm$ beam. We note that the gluon momentum fraction is related to the usual Bjorken-x variable by

$$x_g = x + \frac{\hat{s}}{ys} \geq x \tag{9}$$

For the numerical calculations we use the proton structure functions given by parametrization I of ref. [5] and for the electroweak parameters the following values: $\alpha = 1/137$, $\sin^2\theta_W = 0.226$, $m_W = m_Z\cos\theta_W = 38.68\ GeV/\sin\theta_W$ and $\Delta r = 0.0696$ (c.f. [1]). The Kobayashi-Maskawa matrix elements are chosen as $V_{ud}^2 = 0.95$, $V_{us}^2 = 0.05$, $V_{ub}^2 \leq 10^{-4}$, $V_{cd}^2 = 0.05$, $V_{cs}^2 = 0.948$, $V_{cb}^2 = 0.002$, $V_{td}^2 \leq 4\times10^{-4}$, $V_{ts}^2 = 0.002$, $V_{ud}^2 = 0.998$. The quark masses are taken as $m_s = 0.5$ GeV, $m_c = 1.5$ GeV, $m_b = 5$ GeV and the top quark mass assumed to be $m_t = 60$ GeV unless otherwise stated. The mass scales for the gluon density and for α_s, M_g and M_s, are taken to be $M_g = M_s = \sqrt{\hat{s}}$; the number of flavours, N_f, and Λ_{QCD} in the first order expression for α_s are $N_f = 3, \Lambda_{QCD} = 0.2$ GeV. (These choices are commented below when discussing the uncertainties of our calculations.)

In the following all results are given for an unpolarized electron[1] beam of 30 GeV energy on a 820 GeV proton beam, corresponding to the nominal HERA energy and giving a cms energy $\sqrt{s} = 314$

[1] The $\mathcal{O}(\alpha_s)$ boson gluon fusion cross-sections for unpolarized positron scattering are the same as for electron scattering, only the assignement of quark and antiquark has to be reversed, e.g. instead of $e^-p \to \bar{t}bX$ one has $e^+p \to t\bar{b}X$. The QPM cross-sections are different for electron and positron scattering since different partons within the proton are involved; both cross sections are given for completeness.

GeV. The BGF cross-sections for charm and bottom quarks are given in Table 1 and 2, respectively. For neutral currents, the contributions from pure γ and pure Z^0 exchange as well as their interference are shown separately. The column denoted by 'inclusive' gives the total inclusive cross section for production of the heavy quark or antiquark of flavour f in the BGF model:

$$\sigma_f = 2\sigma(ep \to eQ_f\bar{Q}_f X) + \sum_{f'} \sigma(ep \to \nu Q_f \bar{Q}_{f'} X) \tag{10}$$

These BGF cross-sections should first of all be compared with the corresponding QPM cross sections, obtained from eq. (2), which are also given in Table 1 and 2. As anticipated, charm and bottom quark production through mixing in normal charged current processes, eq. (1), have much smaller cross-sections and can therefore be neglected in the following. For the BGF processes, the NC cross-sections are much larger than the CC ones and hence the charm and bottom production rates via charged current interactions can also be neglected.[2] As seen in Table 1 and 2, the pure γ exchange dominates the weak effects by orders of magnitude. The photon propagator of the γ exchange makes the cross-section dominated by small Q^2 (shown explicitely below) and hence the process corresponds essentially to real photoproduction.

We note that these total cross sections for charm (1μb) and bottom (8.4 nb) are comparable to (or larger than) those expected from Z^0 decays at SLC/LEP: $\sigma_c \approx 7\,\text{nb}$, $\sigma_b \approx 10\,\text{nb}$ [6]. To further illustrate the magnitude of these cross sections we note that with an integrated luminosity of 200 pb^{-1}, corresponding to $\sim$1 year of running at HERA, one would produce about one million bottom and 10^8 charm particles. The high b-rate provides an interesting bottom factory at HERA — if only the events can be experimentally measured, which will be investigated below.

The BGF cross-section for top quark production is shown in Fig. 2 as a function of the unknown top quark mass. In the CC case we restrict ourselves to $\bar{t}b$ production since the other two contributions are negligible, e.g. for $m_t = 60\,\text{GeV}$ we find $\sigma(\bar{t}b) \approx 0.13\,\text{pb}$, whereas $\sigma(\bar{t}s) \approx 0.62 \times 10^{-3}\,\text{pb}$ and $\sigma(\bar{t}d) \leq 0.14 \times 10^{-3}\,\text{pb}$.[3] The corresponding QPM cross sections from eq. (2) are

$$\sigma(t) = V_{td}^2\,\sigma_d + V_{ts}^2\,\sigma_s \leq 4.4 \times 10^{-3} + 7.8 \times 10^{-3} = 1.2 \times 10^{-2}\ \text{pb}$$

$$\sigma(\bar{t}) = V_{td}^2\,\sigma_{\bar{d}} + V_{ts}^2\,\sigma_{\bar{s}} \leq 1.8 \times 10^{-3} + 7.8 \times 10^{-3} = 9.5 \times 10^{-3}\ \text{pb}$$

As for charm and bottom quark production, top production through mixing in normal charged current processes, eq. (1), is so small that it can safely be neglected. Also the contributions from Z^0-exchange and γ-Z^0 interference are negligible as seen in Fig. 2. However, contrary to the charm and bottom cases, top production via the charged current process can *not* be neglected, but actually dominates over neutral current production for $m_t > 55$ GeV due to the reduced threshold for $\bar{t}b$ compared to $t\bar{t}$. For masses above $\sim$85 GeV the top production rate is expected to be below observability at HERA, i.e. less than $\sim$ 10 events for an integrated luminosity of 200 pb^{-1}.

It is interesting to compare with top production in other interactions. In e^+e^- annihilation at SLC and LEP I the top quark should be directly detectable up to 45–50 GeV. However, investigations of B^0-$\bar{B}^0$ mixing by the ARGUS collaboration [7] indicate that the top quark mass is probably heavier than about 50 GeV and the UA1 top search [8] at the CERN $p\bar{p}$ collider puts a lower limit in the range 44–56 GeV depending on uncertainties in the theoretical cross-section calculation. Thus, the main competition for HERA seems to come from future $p\bar{p}$ collider studies. With increase statistics at CERN and the higher energy at the Tevatron a somewhat higher mass region may be reached, but the major problem of large backgrounds makes the top search increasingly difficult. UNK, LHC and

[2] The total cross-sections from the BGF model are not quite safe when light quarks (u, d, s) are involved. Thus the $\bar{c}d$, $\bar{c}s$, $\bar{u}b$, $\bar{t}d$ and $\bar{t}s$ cross sections ($m_u = m_d = 0.3\,\text{GeV}$) should only be considered as rough estimates.

[3] See previous footnote.

SSC are 'post HERA' colliders and we conclude that there is a window of opportunity for top quark discovery at HERA, namely if the top quark mass is in the region 55–85 GeV.

To discuss the limitations of our predictions of heavy flavour production we distinguish between uncertainties within our calculations and possible other production mechanisms. Concerning the latter, we have only considered QPM with mixing and boson-gluon fusion since they are well-defined processes that can give clear predictions and are expected to give a dominant contribution. Other mechanisms are conceivable: an intrinsic charm component in the proton could be probed directly and a hadronic component of the electron would lead to hadronic production processes of heavy flavours (e.g. $gg \to Q\bar{Q}$), diffractive heavy flavour excitation may also be possible. Such processes are, however, not well understood and not constrained enough to allow quantitative predictions. Although these processes may be significant at asymptotic energies, one would expect them to have cross-sections that are much smaller than the BGF process in the HERA energy range.

In order to evaluate the uncertainty in the cross-sections calculated for the boson-gluon fusion process, the chosen parameter values and some ambiguities have to be considered. Since the boson-gluon fusion cross-section formula, eq. (8), is based on the lowest contributing order, $\alpha^2\alpha_s$, in perturbation theory, neither the electroweak coupling constant $\alpha(M^2)$ nor the strong coupling constant $\alpha_s(M_s^2)$ are unambigously defined and we are somewhat free in the choice of the mass scales M^2 and M_s^2 used. Similarly, the mass scale M_g^2 in the gluon structure function, $g(x_g, M_g^2)$, is not well defined. The usual deep inelastic scale Q^2 is clearly not appropriate since the cross-section has important contributions at very small Q^2. Instead we follow ref. [1] and use $\hat{s}$, the invariant squared mass of the $Q\bar{Q}'$-system, for the mass scales of α_s and the gluon density. Reasonable variations of these mass scales lead to uncertainties of the order 10%. For α we use the scale $M^2 = 0$, but note that varying it between zero and the cms energy ($\sqrt{s}$) changes the cross-section by less than 12%. This illustrates the amount of higher order electroweak corrections that can be expected, although these can only partly be taken into account by such a change of the mass scale.

Using different parametrizations of the gluon structure function [5,9] of a conventional type give variations less than 25% for bottom and top production and less than 40% for charm production. A parametrization [10] with a $xg(x) \sim 1/\sqrt{x}$ behaviour at small x increases the charm cross-section by a factor two, but modifies only slightly the bottom and top results since the range in x_g does not extend to as small values, see eq. (11). The number of flavours, N_f, and the value of Λ_{QCD} in the first order expression for α_s are for consistency taken from the structure function parametrization used, i.e. usually $N_f = 3$ and $\Lambda_{QCD} = 0.2$ GeV. For charm and bottom there is the additional uncertainty of the proper definition of the quark masses (current or constituent) and the exact values to use. A decrease of these masses by 0.3 GeV from the assumed ones leads to an increase of the charm and bottom cross-sections by 68% and 22%, respectively, whereas an increase by 0.3 GeV gives a reduction by 36% and 17%, respectively.

Higher order QCD corrections to the boson-gluon fusion process will both change the absolute normalization and influence the event shape (mainly by gluon bremsstrahlung). To get the proper normalisation correction a complete higher order calculation including the virtual corrections would be needed, but since that has not yet been performed K-factors are not easily estimated.[4] We note however, that since it is essentially the heavy quark mass that enter as a cut-off both in the quark propagator (Fig. 1b) and in the argument of $\alpha_s(\hat{s})$ one expects that the result is better the higher the quark mass.[5] The maximum values of the strong coupling constant is 0.26, 0.18 and 0.11 for charm, bottom and top, respectively, which illustrates the possible relative corrections from higher order terms.

[4] As a first step the $\mathcal{O}(\alpha_s^2)$ tree graph contributions were recently calculated [19] in the real photon approximation. With a cut in $p_T(Q\bar{Q})$, to avoid divergences, the corrections to the $Q\bar{Q}$ cross-section turned out to be small; in fact much smaller than the corresponding corrections in hadronic collisions.

[5] This is also the reason why perturbation theory makes sense at all even at low Q^2.

Phenomenological more important is the effect of higher order corrections on the event shape. The main effect, gluon bremsstrahlung off the heavy quark and antiquark, can be approximately taken into account by the use of parton cascade (PC) simulation algorithms. From the experience of jets in e^+e^- annihilation we expect this approach, which includes the leading logarithm contribution of higher corrections, to provide a better description of detailed jet properties, such as hardness and width, as compared to exact next-to-leading order matrix elements. We therefore apply such a cascade algorithm, but note that the rate of clearly separable additional gluon jets does not have to be quite the correct one.

To end the discussion of total cross-sections we show in Fig. 3 the cms energy dependence for the inclusive heavy flavour cross-sections, eq. (10). For charm, which is most sensitive to the gluon structure function the result for a standard parametrization [5] is compared to that from an alternative one with a $xg(x) \sim 1/\sqrt{x}$ behaviour at small x [10]. The latter leads to a substantial increase of the cross-section at larger energies since lower x_g values are then accessible. The corresponding variations for bottom and top (not shown) are considerably smaller due to the larger cutoff in x_g, see eq. (11). The top cross-section is shown for two top quark masses, 50 and 100 GeV. The marked energies correspond to fixed target muon beam experiments at SPS and Fermilab, and ep collisions at HERA and a combination of LEP II and LHC. At HERA there is a strong dependence on the top quark mass since one is still in the threshold region, whereas at higher energies this dependence is reduced. The ratio of top to charm and bottom cross-sections also increases with energy which naturally improves the signal-to-background for a top search. It is therefore clear that finding top at HERA is a difficult task and one needs much more detailed information about the heavy flavour events in order to develope useful analysis procedures.

3 Event kinematics and $Q\bar{Q}$-system variables

Having thus found that heavy quark production cross-sections are large enough to be of experimental interest we now consider some relevant differential distributions and start with the usual DIS kinematical variables for the event as a whole. We recall that only two variables in eq. (5) are independent and can be chosen, e.g., as (x, y) or (x, Q^2). Since the contributions from the QPM mixing processes and all, except one, charged current processes were found to be very small, they are neglected in the following. Thus we consider only $\bar{t}b$ production in the charged current case, whereas all NC processes $(c\bar{c}, b\bar{b}, t\bar{t})$ are included in the following analysis; all in e^-p scattering at HERA energy.

The Q^2-dependence is shown in Fig. 4a. Note that $d\sigma/d\log Q^2 = Q^2\, d\sigma/dQ^2$ is given, such that in the NC case the effective Q^{-2} dependence at low Q^2 from the photon exchange process is cancelled leading to an essentially flat curve at small Q^2. The lower limit is at exceedingly small values of Q^2 since it is governed by the electron mass, but also increases with the heavy quark mass $\approx m_e^2(m_Q + m_{\bar{Q}'})^4)/s^2$. Thus, for the neutral current case the bulk of the cross-section is in the region of almost on-shell photon exchange, i.e. photoproduction, and hence the Weizäcker-Williams (equivalent photon) approximation can be used as a good approximation [1]. In the charged current case, however, the cross-section has important contributions at larger Q^2 due to the exchange of the massive W-boson. The dependence on Q^2 is reflected in the angle of the scattered lepton, Fig. 4b. Thus, for NC events the scattered electron is dominantly at very small angles so that its detection would require a very forward detector which is integrated with the machine magnet elements to bend the (lower energy) scattered electron out of the beam.

Fig. 5 display the relative variation of the double differential cross-section $d\sigma/d\log x dy$ and shows that all NC processes are dominantly at small x as a reflection of the Q^2 dependence. The cross-section is also peaked at small y for charm, but shifts to larger y with increasing quark mass. The charged

current $\bar{t}b$ events are dominantly located at moderate x and cover a rather large region in y. It should be noted that in the region defined by $10^{-2} < x < 1$ and $0.4 < y < 1$, $\bar{t}b$ production is actually close to 1% of the total CC deep inelastic cross-section.

Considering now the $Q\bar{Q}'$ system, we show the distribution of its invariant mass, $\sqrt{\hat{s}}$, in Fig. 6a. The cross-section dominates close to threshold and falls steeply above. For this reason it is essential to have the proper mass-dependence included in the matrix elements. The invariant mass W of the complete hadronic system has a rather different distribution, Fig. 6b, due to the addition of the target remnant [11]. A cut in W is not effective in separating the heavier flavours bottom and top from the dominant charm production whereas a cut in $\hat{s}$ would be better. On the other hand $\hat{s}$ is more difficult to measure experimentally.

The momentum fraction, x_g, of the gluon is an interesting variable since it can give information on the gluon structure function. For the purpose of extracting the gluon density, heavy quark production in ep collisions has the advantage that the gluon density (and only the gluon density) enters already at the Born level since the production mechanism is dominantly given by BGF. The distributions in x_g for the heavy flavour processes are shown in Fig. 7 and compared with the original gluon distribution used as input in the calculation. All curves are normalised to unit area for easier comparison. The kinematical lower limit

$$x_g \geq \frac{(m_Q + m_{\bar{Q}'})^2 + Q^2}{ys} \tag{11}$$

is small for charm and bottom production, but significant for top as seen directly in Fig. 7. For charm, x_g is always larger than 10^{-4} and hence typically $x_g \gg x$, eq. (9). Although the gluon structure function parametrization is unreliable for x_g as small as 10^{-4}, the charm cross section does not vary drastically, e.g. an extra $1/\sqrt{x_g}$ in the gluon density changes the charm cross section by a factor of two only, see Fig. 3. Since the cross-section in eq. (8) depends on both the gluon distribution and the QCD matrix element, the extent to which the shape of these curves agree with the gluon distribution depends on the QCD part. Naturally, the more similar the shape the easier to extract the gluon structure function and in this respect the results in Fig. 7 are promising. From the experimental point of view, however, the variable x_g is not directly accessible and its reconstruction through eq. (9) depends on the ability to determine $\hat{s}$, a subject which needs a dedicated study.

4 Heavy Quark and Hadron Distributions

The formalism in Section 2 is only sufficient to calculate properties at the parton level in leading order QCD, but to obtain a realistic description of the final hadronic state models for jet evolution and hadronization must be added [12]. Although the proper higher order QCD corrections to the boson-gluon fusion process have not yet been calculated one can take their effect on the final state, but not on the overall cross-section, approximately into account by the parton cascade approach. Similarly to the $q\bar{q}$ pair produced in e^+e^- annihilation the heavy $Q\bar{Q}'$ pair can emit bremsstrahlung gluons (some of which may split perturbatively into gluon or $q\bar{q}$ pairs) thereby creating a cascade at the parton level and we therefore apply the model for e^+e^- [3] to simulate this in our case as well. In doing so an uncertainty arises as to what scale to use for the maximum offshellness of the heavy quark and antiquark that initiate the cascade. A first choice would be $\hat{s}$. This particular cascade algorithm is, however, constructed to give more hard gluon emission than the order α_s matrix element in e^+e^- such that the matrix element can be used as a weighting factor to get the correct first order result. A similar procedure would be possible in our case if the next-to-leading order matrix elements were known and could be matched with the cascade. Since this is an unsolved, complicated problem we instead argue that similarly to the $gg \to Q\bar{Q}$ process in hadron collisions one should use a measure of the momentum transfer, rather than the invariant mass, and we therefore choose the scale as $(m_{\perp Q} + m_{\perp \bar{Q}'})^2$. In

practice, however, the differences arising from these, and other similar, scales are small so that the exact scale choice is not very important. In particular, we have verified that the use of $\hat{s}$ as the scale and applying the matrix element rejection from $\mathcal{O}(\alpha_s)$ e^+e^-, gives essentially the same distribution in offshell quark mass (Fig. 12) and hence the resulting phenomenology is left unchanged. Having thus generated a multiparton final state, including the target remnant [13,11], we apply the Lund string model [4,3] for the final hadronization step. Thus we obtain a Monte Carlo model for heavy flavour production in ep collisions that generates complete events with the full information on both the parton and the hadron level. In this computer program, AROMA version 1.2 [2], the physics input and parameters values are as given in Section 2.

The rapidity and transverse momentum distributions of the heavy quark and resulting heavy hadrons (in the HERA laboratory frame) are shown in Fig. 8 and 9, respectively. The different sets of curves are for $c\bar{c}, b\bar{b}, t\bar{t}$ and $\bar{t}b$ events separately, i.e. without any feed-down from heavier flavours in the other events which are also negligible due to the large differences in cross-section scales. The curves shown for the hadrons include all mesons and baryons that are stable against strong and electromagnetic decays. The baryons are dominantly formed by diquark pair production [14] in the string breaking and are suppressed by an order of magnitude compared to the mesons, but have similar forms of the distributions. An exception is seen in the charm case for large negative rapidities (proton direction) where a recombination with a spectator diquark [15] gives a relatively larger baryon yield seen as the 'bump' on the curve (marked D); for heavier quarks this effect is less pronounced and not directly seen.

The gluon radiation off the heavy quark reduces its momentum as shown by the curves before and after gluon radiation in Fig. 9. Due to the similar losses in both energy and momentum the rapidity is essentially unchanged giving overlapping curves which are not both shown in Fig. 8. One should note the reduced effect of the gluon radiation with increasing quark mass. This is due to the reduced phase space, given by $\log(m_Q^*/m_Q)$, for radiation between the upper and lower limits of the quark virtuality, i.e. the initial offshell mass and the onshell quark mass.

The fragmentation function for charmed mesons has been observed [16] to be considerably harder than for light mesons and still harder for bottom mesons as can be well reproduced by the symmetric fragmentation scheme in the Lund model [17], which predicts the fragmentation function

$$f(z) = \frac{(1-z)^a}{z} \, exp\left\{-bm_\perp^2/z\right\} \tag{12}$$

where z is the energy-momentum fraction of the hadron compared to the quark. The appearance of the hadron transverse mass, $m_\perp$, suppress small z values for heavy hadrons making the spectrum increasingly harder with increasing mass. Asymptotically $<1-z>=(a+1)/bm^2$ in this model which is harder than the $1/m$ dependence obtained by simple arguments [18]. Thus, with increasing heavy quark mass, the hadron spectra approach the quark ones as can be clearly seen in Figs. 8 and 9. The top quark and hadron rapidity curves overlap, whereas the charm and bottom hadrons are at slightly more negative rapidities compared to the quarks. This shift is caused by the fragmentation of the two colour singlet systems composed of the heavy quark and a spectator diquark from the target remnant joined by one colour triplet string, and the heavy antiquark and a spectator quark joined by another [13,11].

A few experimental consequences are immediately clear from these distributions. The most important fact is that most of the cross-section is concentrated at rather central rapidities and thus most of the heavy flavours emerge in a region covered by normal detectors, i.e. $-3.5 \lesssim y_{lab} \lesssim 2$. Only for charm there is a substantial fraction boosted 'down the beam pipe' in the proton direction. On the other hand, a simple cut in rapidity has no effect in enhancing bottom and top samples at the expense of charm events. Concerning the transverse momentum one should note that the distributions are

strongly suppressed only for values above the corresponding quark mass, since only then $\hat{s}$ is significantly increased. Strictly speaking this only applies in the boson-gluon CM frame, but for the neutral current case, which is dominated by low Q^2, there is no strong transverse boost between this frame and the laboratory frame (used in Fig. 9). We thus obtain significantly increasing mean transverse momenta in the sequence charm–bottom–top hadrons.

5 Heavy Flavour Signatures

Although the mean transverse momentum is larger for heavier quarks one also has to consider the absolute normalisation of the long tails at large $p_\perp$ that occur also for the lighter flavours. This comparison is made in Fig. 10a for charm, bottom and top mesons from $c\bar{c}$, $b\bar{b}$ and $t\bar{t}+\bar{t}b$, respectively, and shows that the cross-over points are at very large $p_\perp$. These long tails are due to a normal power dependence of the quark and antiquark in the hard $Vg \to /Q\bar{Q}$ subprocess. The heavy mesons themselves are, furthermore, not easily reconstructed and one would rather try to look for observable signatures in their decay products. A standard such is the detection of muons from semileptonic heavy flavour decays. Fig. 10b shows the $p_\perp$ spectra of the inclusive $\mu^\pm$ from charm, bottom and top decays in these event classes. Note that muons from sequential bottom and charm decays are included in the top case and correspondingly charm decays are included in the bottom case. These sequential decays give in each case a contribution in the lower $p_\perp$ region only. The cross-over point between muons from charm and bottom events is at relatively small $p_\perp$ ($\approx$ 4 GeV) and can therefore provide a bottom sample of large statistics. A lepton $p_\perp$-cut could also be used to obtain a top sample, but in order to have a non-vanishing statistical sample the cut cannot be made too large and the charm/bottom background is therefore always disturbingly large. We note that without the softening of the charm and bottom quark momentum due to gluon radiation (Fig. 9) their decay muons would have been even harder and thus have given an even more severe background for a top search. In spite of this background, a lepton $p_\perp$-cut should be very useful in combination with other criteria to obtain a clean top event sample.

From the increasing transverse momenta with increasing quark mass together with the larger energy release in their decays one also expects an increasing global transverse energy for heavier flavours. This is indeed the case, as is shown by the distribution of total transverse energy, $\sum E_\perp$, in Fig. 11. All stable (charged and neutral) particles outside a beam-pipe cut of 4^0 are here included in order to correspond to a straightforward measurement of total transverse energy in a calorimeter. The orders of magnitude larger scales of the charm and bottom cross-sections do, however, give rise to long tails which are always above the corresponding curve for top events. Nevertheless, a cut in this variable can be used to substantially reduce the charm and bottom contributions, but only reject a small fraction of the top events.

Due to the large energy available in the top quark decay one would also expect the top events to be more spherical than charm and bottom events. In average this is also correct, but again the charm and bottom events have tails to large sphericities that completely mask the top events when the absolute cross-section is taken into account. Since the events in ep collisions do not only include the $Q\bar{Q}'$ system but also the target remnant, it makes more sense to suppress the latter by applying the sphericity analysis in the transverse plane only. This transverse sphericity is then rather a measure of 'circularity' which can be defined by $C = 2\lambda_2$ in terms of the smaller eigenvalue, λ_2, of the two-dimensional sphericity tensor ($S_{\alpha\beta} = \sum_i p_{i\alpha}p_{i\beta} / \sum_i p_i^2$ where α, β are Cartesian components and i runs over the particles in the event). The distribution in circularity for the inclusive charm plus bottom event sample is compared with the one for all top events in Fig. 13. The charm/bottom events are, somewhat surprisingly, quite circular and orders of magnitude above the top events. The reason for this behaviour of the charm and bottom events is twofold. Firstly, they are dominantly produced close

to threshold (Fig. 6a), i.e. without significant transverse momentum, and therefore decay in a rather isotropic way. Secondly, when the charm and bottom quarks have large transverse momenta they do not produce very pencil-like jets because of the gluon radiation. As mentioned, the heavy quark transverse momentum sets the scale for the offshellness of the heavy quark which in turn regulates the gluon emission. This leads to the distribution in offshell masses of the different heavy quarks shown in Fig. 12. As can be seen, the offshell masses of charm and bottom quarks extend to values well above the physical top quark mass. This makes a top search based on invariant masses of combinations of jets non-trivial since also the lighter flavours will produce multijet events with large such masses. The top quark mass spectrum has a peak at its physical value which could in principle be used for a top search. One should realise, however, that the exact shape given in Fig. 12 depends somewhat on details of the parton cascade algorithm. Furthermore, jet mass reconstruction is a difficult subject where large smearing effects can arise due to both experimental resolution and the analysis procedure.

In spite of the gluon radiation effects, which are only of a logarithmic nature, jets are becoming narrower with increasing energy [12]. The expected difference in circularity, between gluon radiation effects in charm and bottom events and weak decay effects in top events, should therefore be observed more clearly for events with a large transverse energy. (Since this forces the charm and bottom quarks to have large transverse momenta.) Fig. 13 also shows the resulting distribution of circularity when applying a cut $\sum E_\perp > 100$ GeV on the total transverse energy, see Fig. 11. A top signal is now seen to stand out above the background. This signal for $C > 0.35$ corresponds to a cross-section of 1.8×10^{-2} pb, whereas the corresponding number for charm plus bottom is 1.0×10^{-2} pb. Thus, such a large $E_\perp$-cut also removes a significant part of the top events as is clear from Fig. 11. Practically the complete CC cross-section is lost, leaving only a few $t\bar{t}$ events per year of data taking. Nevertheless, we have demonstrated that a top signal can be obtained, but it may be more promising to lower the $E_\perp$-cut somewhat, still using its strong discriminating power against the lighter flavours, to leave a larger sample of top events. The increased background would then have to be removed by other selection criteria which could, however, be more sophisticated since only a small event sample would have to be carefully investigated. Various types of topologies, involving multijets and leptons, could be used for this purpose, but this requires a detailed study beyond the scope of this paper.

We remark that for this first exploratory study of heavy flavour signals we have not taken all background processes into account. Since the signatures always involve requirements of large transverse momenta, most processes with large cross-sections are effectively suppressed, e.g. photoproduction in the VDM approach. The major additional physics background is therefore expected to arise from the low-Q^2 photoproduction processes of photon-gluon fusion into light flavours (u, d, s) and from the QCD Compton process $\gamma q \rightarrow qg$. As mentioned, only configurations where the final partons emerge at large $\mathrm{p}_\perp$ are of interest and the corresponding cross-sections are therefore suppressed to a level comparable to that for $\gamma g \rightarrow c\bar{c}$ at large $\mathrm{p}_\perp$. In fact, our boson-gluon fusion Monte Carlo generator is also applicable to the case of light flavours provided that a lower cut in $\mathrm{p}_\perp$ is applied. We have thus verified that the cross-sections are indeed close to the charm ones (modulo quark charges) for a $\mathrm{p}_{\perp cut}$ larger than a few GeV where the quark mass is negligible compared to the transverse momentum. The QCD Compton process has a cross-section of similar magnitude and, although the final parton state is somewhat different, the main event characteristics are also expected to be similar and these events should therefore respond similarly to the cuts which were applied to reject the charm events. The deep inelastic events ($Q^2 \gtrsim 1$ GeV^2) will only contribute for large Q^2, since only then large $\mathrm{p}_\perp$ particles are generated. This implies a reduced cross-section. Furthermore, these events should have a clearly different topology; the high-$\mathrm{p}_\perp$ hadron system is in one azimuthal hemisphere opposite to the scattered lepton. Such events should therefore be easily separable from the more symmetric heavy flavour events. We thus conclude that the only important additional background processes are similar to the $c\bar{c}$ background already considered and will only produce an increase by a limited factor, not by orders of magnitude.

6 Discussion

To summarize we have constructed a complete model for heavy flavour production in *ep* collisions via the boson-gluon fusion mechanism. Multiple gluon emission, hadronization (including the target remnant) and heavy flavour decays are built in to simulate the complete final state. The overall cross-sections at HERA energy are very large for charm and bottom, and large enough for top quark production to give an interesting rate up to a top mass of ~85 GeV. Neutral current events dominate the production of charm and bottom and also top if the top quark mass is below 50 GeV. Due to the dominance of photon exchange in this case, the events are concentrated at very low Q^2 such that the scattered electron mostly appear at very small angles and is therefore difficult, if not impossible, to measure. Thus, one would usually not have access to the normal deep inelastic variables from the scattered electron, but a reconstruction from the hadronic system using the Jacquet-Blondel method can be made, as for charged current events, provided that the net transverse momentum is not too small. The produced heavy flavours emerge mostly in a region of phase space which is covered by the detector arrangements in the experiments at HERA, thus making their detection possible.

The typical transverse momentum scale is given by the mass of the produced quark. This leads to possible selection criteria for bottom and top events. There are, however, long tails to large transverse momenta for charm and bottom events which complicate such a selection. For example, although the mean total transverse energy is much larger for top events, the tails from the orders of magnitude larger charm and bottom cross-sections mask the top events also at very large $\sum E_\perp$. The gluon radiation, off the heavy quark and antiquark, gives a softening of the momentum spectra. This effect is less important the heavier the quark mass and hence charm distributions are significantly influenced, bottom less and top left almost unchanged. This effect is enforced by the increasingly harder fragmentation function for heavier quarks which make the top quark and hadron distributions virtually identical. The simple signature in terms of large $p_\perp$ muons is useful to obtain a bottom sample, but not quite efficient to obtain a clean top sample with reasonable statistics and should therefore be combined with other top selection criteria. A cut in total transverse energy is very efficient in reducing the charm and bottom background in a top sample, but cannot make a clean selection in itself. Combined with event shape measures of the sphericity type one can obtain a decent sample which can be carefully investigated with respect to jet topologies and lepton signatures to find the precious top events. It is clear from our study that there is no single observable that can separate the top events from the huge background. A successful top search has, therefore, to be based on the combination of several selection criteria. This requires a dedicated study taking additional backgrounds as well as experimental limitations into account.

Due to the large charm and bottom cross-sections it should be possible to get rather clean such event samples, e.g. through lepton signatures, which can be used for detailed tests of various aspects of heavy flavour production. The QCD matrix elements for the boson-gluon fusion process can be compared in detail with the data and one could attempt to extract the gluon structure function. Depending on the experimental possibility to reconstruct bottom decays, subjects like life-times, branching ratios and mixing could also be investigated. It is therefore clear that heavy flavour physics in *ep* collisions is an interesting field which has a potential to yield a rich harvest.

Acknowledgements. We are grateful to Drs. A. Ali and F. Barrerio for interesting and helpful discussions.

References

[1] G.A. Schuler, DESY 87–114, Nucl. Physics B in press

[2] G. Ingelman, G.A. Schuler, AROMA 1.2 – A Generator of Heavy Flavour Events in *ep* Collisions, DESY preprint in preparation

[3] M. Bengtsson, T. Sjöstrand, Comput. Phys. Common. 43 (1987) 367

[4] B. Andersson, G. Gustafson, G. Ingelman, T. Sjöstrand, Phys. Rep. 97 (1983) 31

[5] E. Eichten, I. Hinchliffe, K. Lane, C. Quigg, Rev. Mod. Phys. 56 (1984) 579, ibid. 58 (1986) 1047

[6] A. Ali, proc. workshop on Physics at LEP, Eds. J. Ellis, R. Peccei, CERN 86-02, Vol. 2, p. 220

[7] H. Albrecht et al., ARGUS collaboration, Phys. Lett. 192B (1987) 245

[8] C. Albajar et al., UA1 collaboration, CERN-EP/87-190

[9] D.W. Duke, J.F. Owens, Phys. Rev. D30 (1984) 49
M. Glück, E. Hoffman, E. Reya, Z. Phys. C13 (1982) 119

[10] A.D. Martin, R.G. Roberts, W.J. Stirling, Rutherford preprint RAL-87-052

[11] G. Ingelman, LEPTO 5.2, DESY preprint in preparation

[12] G. Ingelman, DESY 87–145 and proc. XVth International Winter Meeting on Fundamental Physics, Sevilla, Spain, 1987

[13] B. Andersson, G. Gustafson, G. Ingelman, T. Sjöstrand, Z. Phys. C13 (1982) 361

[14] B. Andersson, G. Gustafson, T. Sjöstrand, Phys. Scripta 32 (1985) 374

[15] B. Andersson, H.U. Bengtsson, G. Gustafson, Lund preprint LU TP 83-4

[16] For a review see
S. Bethke, Z. Phys. C29 (1985) 175

[17] B. Andersson, G. Gustafson, B. Söderberg, Z. Phys. C20 (1983) 317
For a comparison with data see
G. Ingelman, proc. XV International Symposium on Multiparticle Dynamics, Lund 1984, World Scientific, Eds. G. Gustafson, C. Peterson, p. 664

[18] J.D. Bjorken, Phys. Rev. D17 (1978) 171

[19] R.K. Ellis, Z. Kunszt, Fermilab preprint, FERMILAB-Pub-87/226-T December, 1987

Table 1

$\sigma(ep \to cX)$ [pb] at HERA ($m_c = 1.5\,\text{GeV}$)								
	CC			NC $c\bar{c}$				inclusive
e^-p	$\bar{c}d$	$\bar{c}s$	$\bar{c}b$	NC	γ	Z	γ-Z	$c + \bar{c}$
BGF	0.46	8.2	0.012	5.1×10^5	5.1×10^5	0.60	4.7	1.0×10^6
e^-p	$\bar{d} \to \bar{c}$	$\bar{s} \to \bar{c}$						
QPM	0.26	3.3						3.6
e^+p	$d \to c$	$s \to c$						
QPM	0.75	3.3						4.1

Table 2

$\sigma(ep \to bX)$ [pb] at HERA ($m_b = 5\,\text{GeV}$)								
	CC			NC $b\bar{b}$				inclusive
e^-p	$\bar{u}b$	$\bar{c}b$	$\bar{t}b$	total	γ	Z	γ-Z	$b + \bar{b}$
BGF	$\leq 0.96 \times 10^{-3}$	0.012	0.13	4.2×10^3	4.2×10^3	0.35	0.59	8.4×10^3
e^-p	$u \to b$							
QPM	$\leq 0.56 \times 10^{-2}$							$\leq 0.56 \times 10^{-2}$
e^+p	$\bar{u} \to \bar{b}$							
QPM	$\leq 0.12 \times 10^{-2}$							$\leq 0.12 \times 10^{-2}$

Figure captions

Figure 1 (a) Normal charged current interaction with flavour mixing giving a single heavy quark. (b) First order QCD diagrams for boson-gluon fusion into a heavy quark-antiquark pair.

Figure 2 Cross-section for top quark production via boson-gluon fusion as a function of the top quark mass. The curves are for $\bar{t}b$ production in charged current interactions (W), and for $t\bar{t}$ production in the neutral current case separately for pure γ, pure Z and their interference $\gamma - Z$. The inclusive cross-section is for $t + \bar{t}$ as defined in eq. (10).

Figure 3 Inclusive heavy flavour cross-section, eq. (10), as a function of the ep cms energy. The curves for charm are for two alternative structure functions [5,10] and those for top correspond to a top quark mass of 50 and 100 GeV, respectively. Energies for fixed target muon beam experiments at CERN and Fermilab are indicated as well as ep collisions in HERA and a combination of LEP II and LHC.

Figure 4 (a) Q^2 dependence of the cross-sections for neutral current production of $c\bar{c}$, $b\bar{b}$ and $t\bar{t}$, and charged current production of $\bar{t}b$. (b) Laboratory angle of the scattered lepton. Curves as in (a). (Base 10 logarithm is used.)

Figure 5 Relative variation of the cross-section in the $\log x, y$ plane, i.e. $d\sigma/d\log x dy$, for $c\bar{c}$, $b\bar{b}$, $t\bar{t}$ and $\bar{t}b$.

Figure 6 Dependence of cross-section on (a) the invariant mass, $\sqrt{\hat{s}}$, of the heavy quark-antiquark system, and (b) the invariant mass, W, of the total hadronic system including the target remnant.

Figure 7 Momentum fraction, x_g, of the initial gluon with respect to the proton for the $c\bar{c}$, $b\bar{b}$, $t\bar{t}$ and $\bar{t}b$ production processes in comparison to the gluon structure function used as input in eq. (8); this long-dashed curve corresponds to $g(x, Q^2 = 4m_b^2)$ from [5]. All curves are normalised to unit area.

Figure 8 Rapidity distribution of heavy quarks and hadrons (sum of mesons and baryons of the corresponding flavour) in the laboratory frame of HERA. The separate sets of curves are for $c\bar{c}$, $b\bar{b}$, $t\bar{t}$ and $\bar{t}b$ production, respectively. (Top quark and hadron curves overlap.)

Figure 9 Transverse momentum in the HERA lab frame for the heavy quark before (dashed) and after parton shower gluon emission (dotted), and for the corresponding hadrons after string fragmentation (full).

Figure 10 Transverse momentum distributions for (a) charm, bottom and top mesons in $c\bar{c}, b\bar{b}, t\bar{t} + \bar{t}b$ production, respectively, and (b) muons from (any) heavy flavour decay in the corresponding cases.

Figure 11 Distribution of the total transverse energy, $\sum E_\perp$, of all stable particles outside a beam pipe cone of 4^0, with curves corresponding to $c\bar{c}, b\bar{b}, t\bar{t}$ and $\bar{t}b$ events.

Figure 12 Distribution in offshell mass, m_Q^*, of the quark initiating the parton cascade evolution. The curves are for charm quarks in $c\bar{c}$ events (dotted), bottom quarks in $b\bar{b}$ (full), top quarks in $t\bar{t}$ (dashed) and in $\bar{t}b$ (dash-dotted).

Figure 13 Distribution of circularity, i.e. sphericity in the transverse plane, with C=1 corresponding to a circularly symmetric final state and C=0 to a back-to-back pencil-like two-jet system. The curves correspond to inclusive samples of $c\bar{c} + b\bar{b}$ events (dotted) and $t\bar{t} + \bar{t}b$ events (dashed). The corresponding subsamples defined by requiring a total transverse energy larger than 100 GeV are also shown, i.e. the charm+bottom background (dash-dotted) and the top signal (full curve).

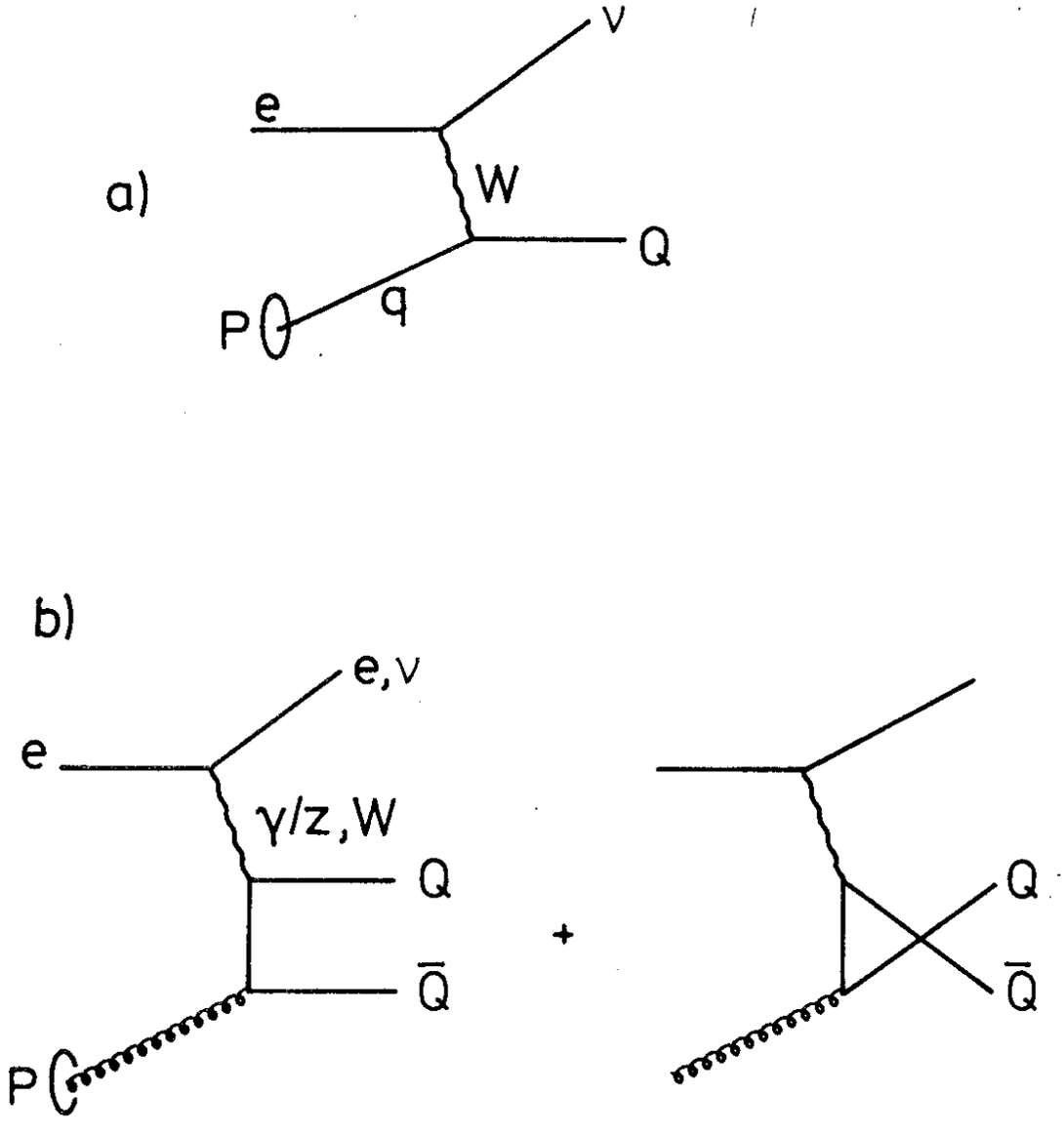

Fig.1

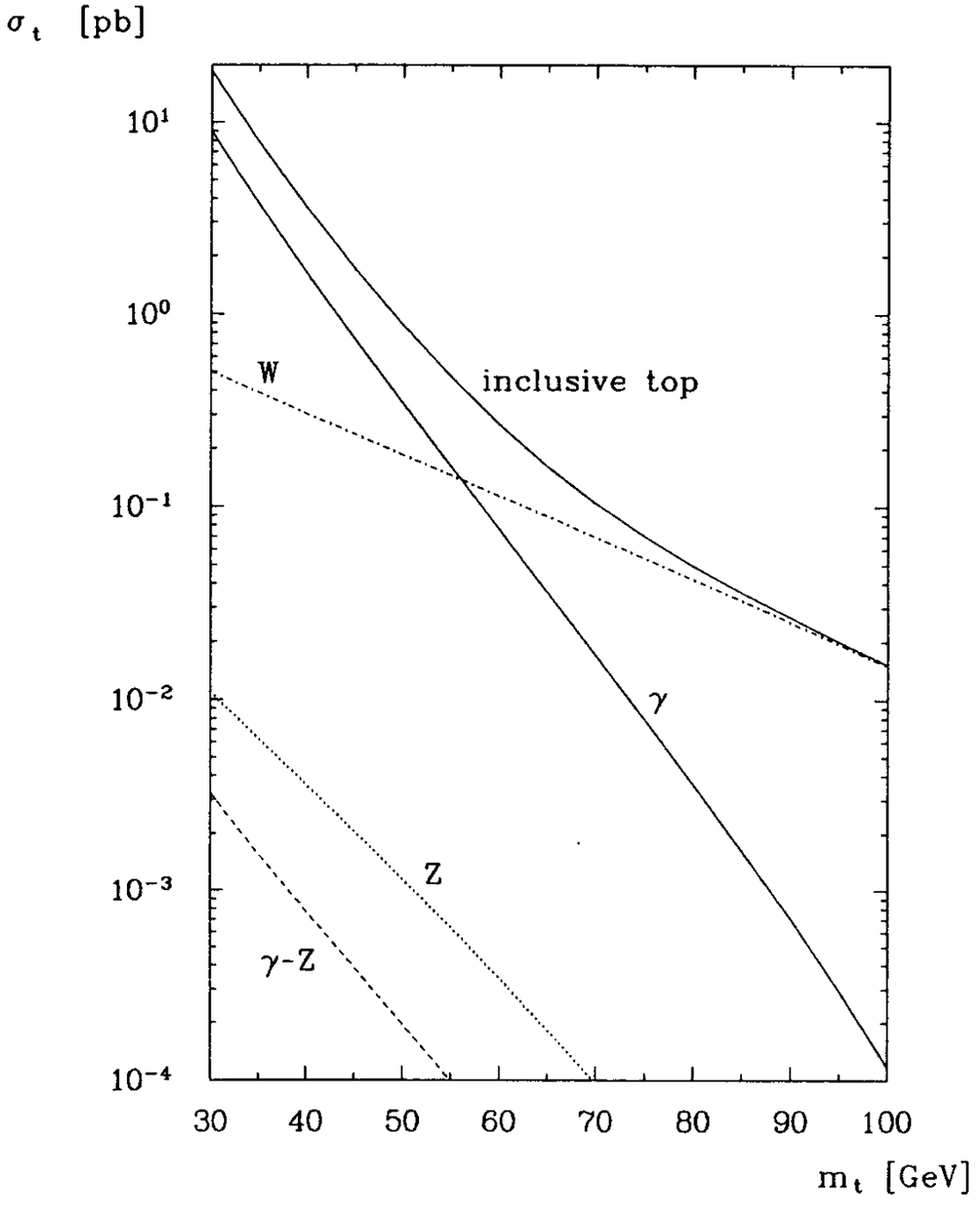
σ_t [pb]
10^1
10^0
10^{-1}
10^{-2}
10^{-3}
10^{-4}
W
inclusive top
γ
Z
γ-Z
30
40
50
60
70
80
90
100
m_t [GeV]

Fig. 2

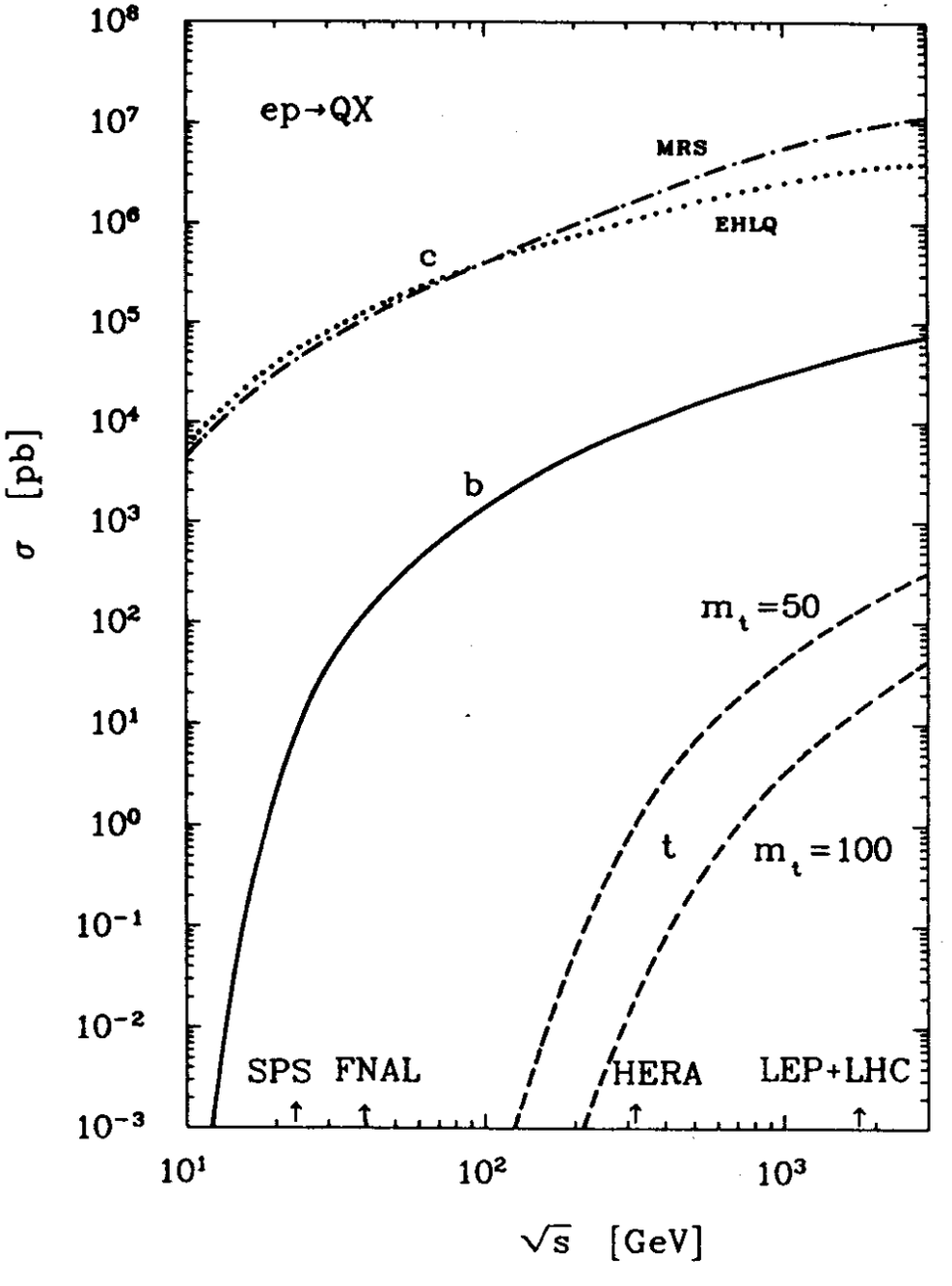
10^8
10^7
10^6
10^5
10^4
10^3
10^2
10^1
10^0
10^{-1}
10^{-2}
10^{-3}
ep→QX
MRS
EHLQ
c
b
m_t=50
t
m_t=100
SPS FNAL
HERA
LEP+LHC
10^1
10^2
10^3
σ [pb]
$\sqrt{s}$ [GeV]

Fig. 3

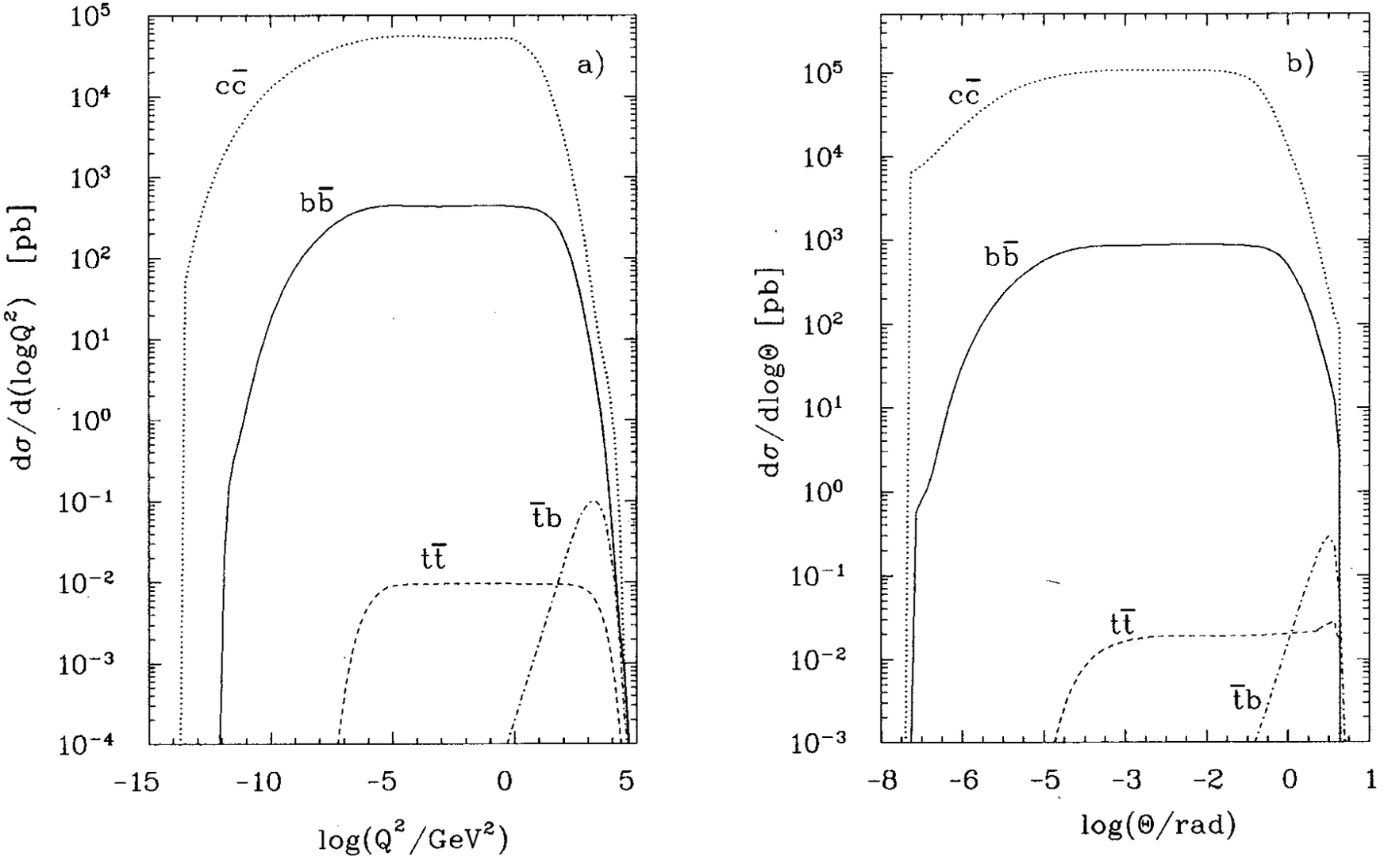
a)
b)
$c\bar{c}$
$b\bar{b}$
$t\bar{t}$
$\bar{t}b$
$d\sigma/d(\log Q^2)$ [pb]
$d\sigma/d\log\Theta$ [pb]
$\log(Q^2/\mathrm{GeV}^2)$
$\log(\Theta/\mathrm{rad})$

Fig. 4

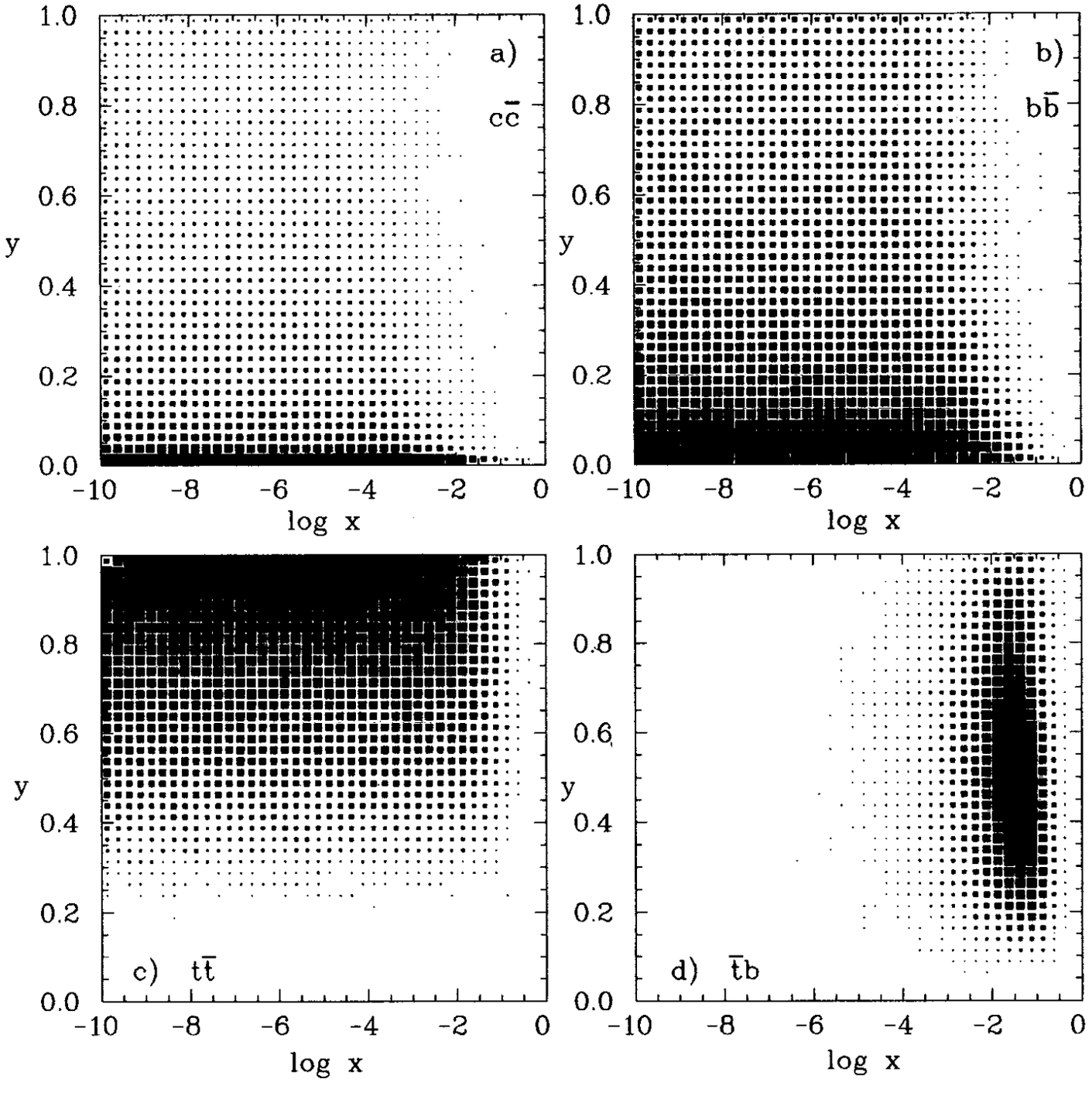

Fig. 5

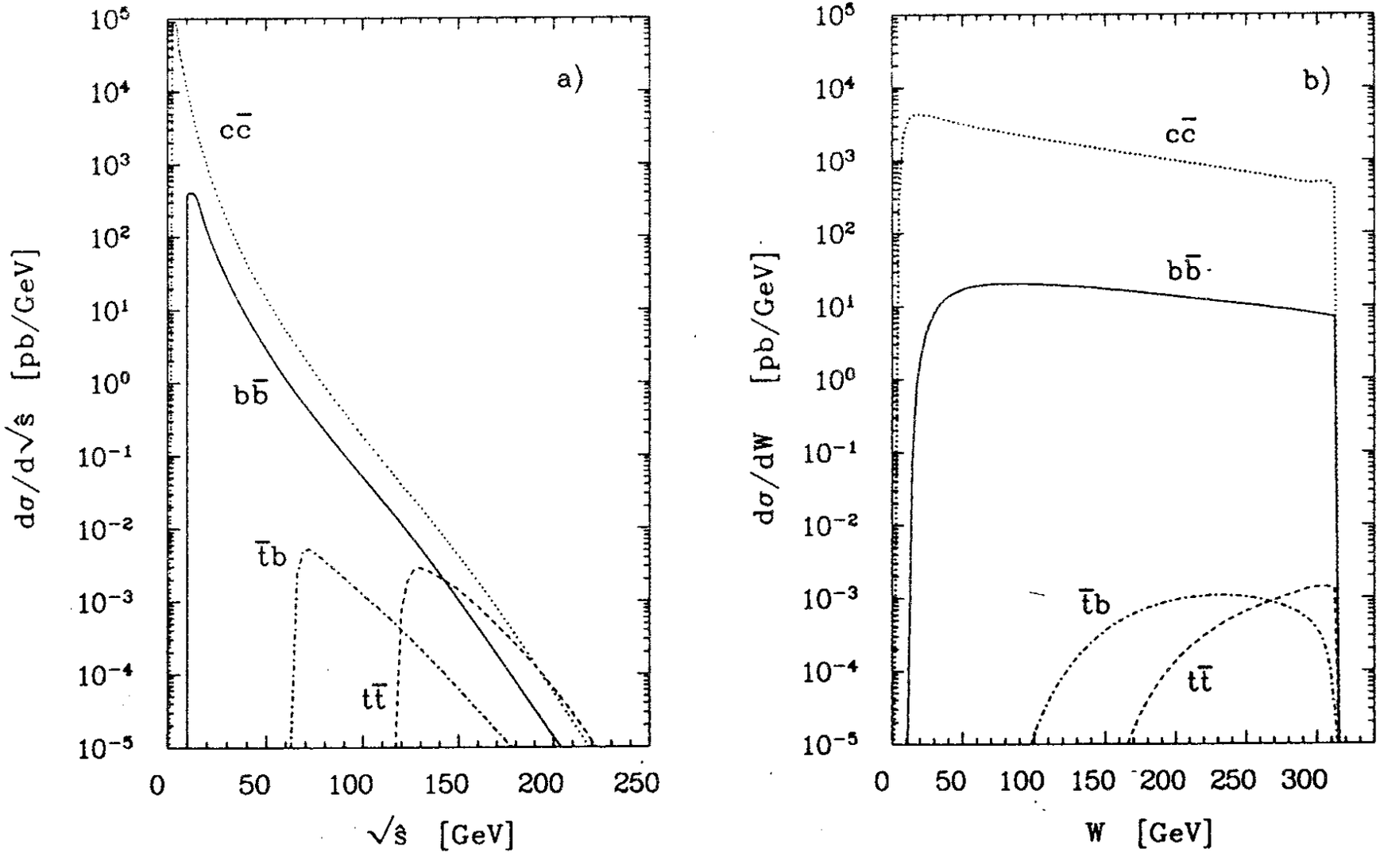
a)
b)
$c\bar{c}$
$b\bar{b}$
$\bar{t}b$
$t\bar{t}$
$d\sigma/d\sqrt{\hat{s}}$ [pb/GeV]
$d\sigma/dW$ [pb/GeV]
$\sqrt{\hat{s}}$ [GeV]
W [GeV]
10^5
10^4
10^3
10^2
10^1
10^0
10^{-1}
10^{-2}
10^{-3}
10^{-4}
10^{-5}
0
50
100
150
200
250
300

Fig. 6

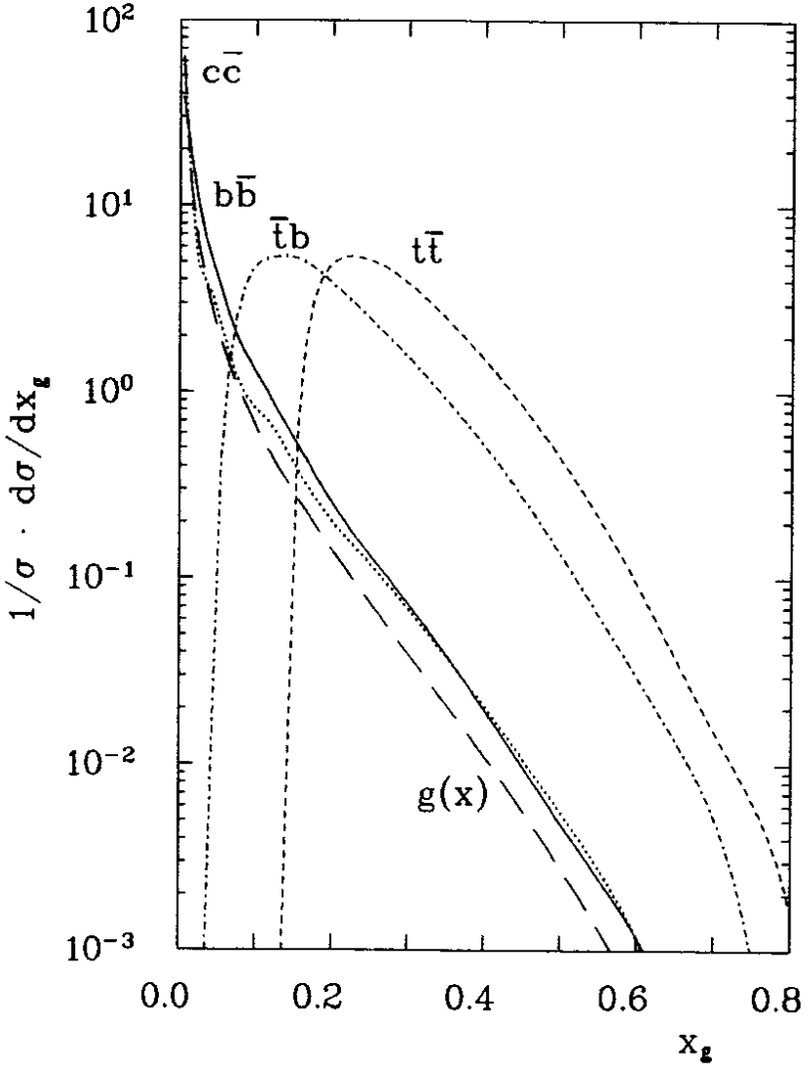
10^2
10^1
10^0
10^{-1}
10^{-2}
10^{-3}
$1/\sigma \cdot d\sigma/dx_g$
$c\bar{c}$
$b\bar{b}$
$\bar{t}b$
$t\bar{t}$
g(x)
0.0
0.2
0.4
0.6
0.8
x_g

Fig. 7

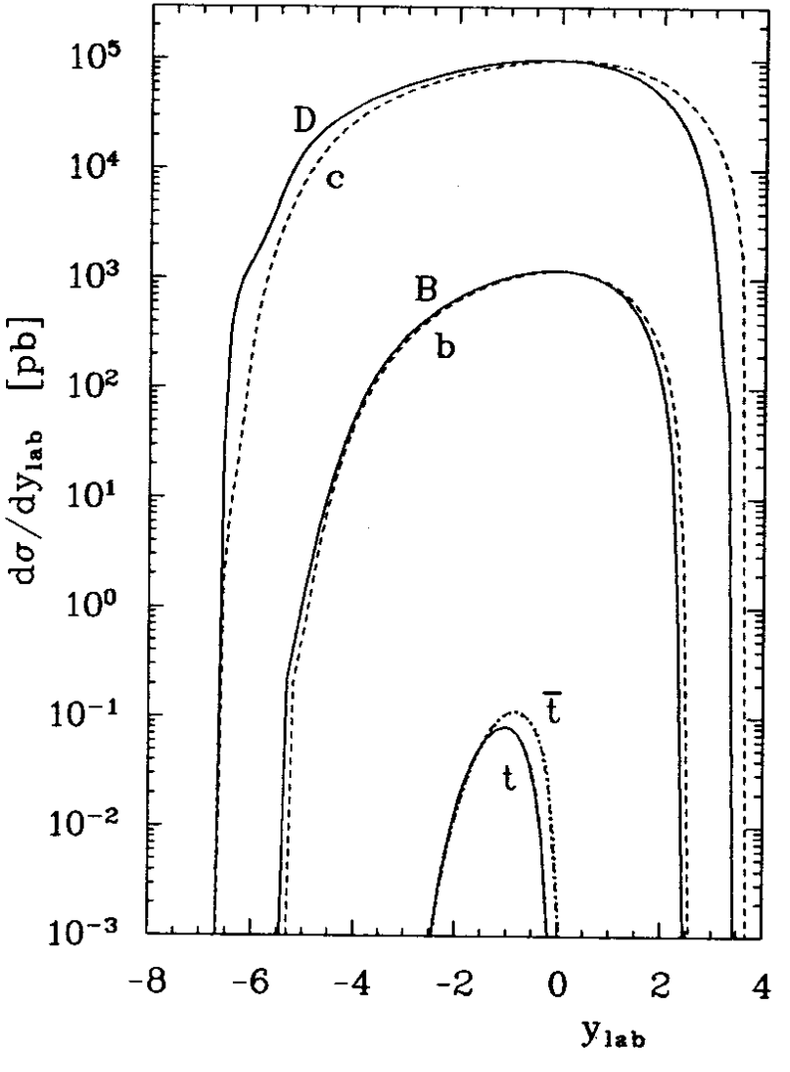
10^5
10^4
10^3
10^2
10^1
10^0
10^{-1}
10^{-2}
10^{-3}
$d\sigma/dy_{lab}$ [pb]
D
c
B
b
$\bar{t}$
t
-8
-6
-4
-2
0
2
4
y_{lab}

Fig. 8

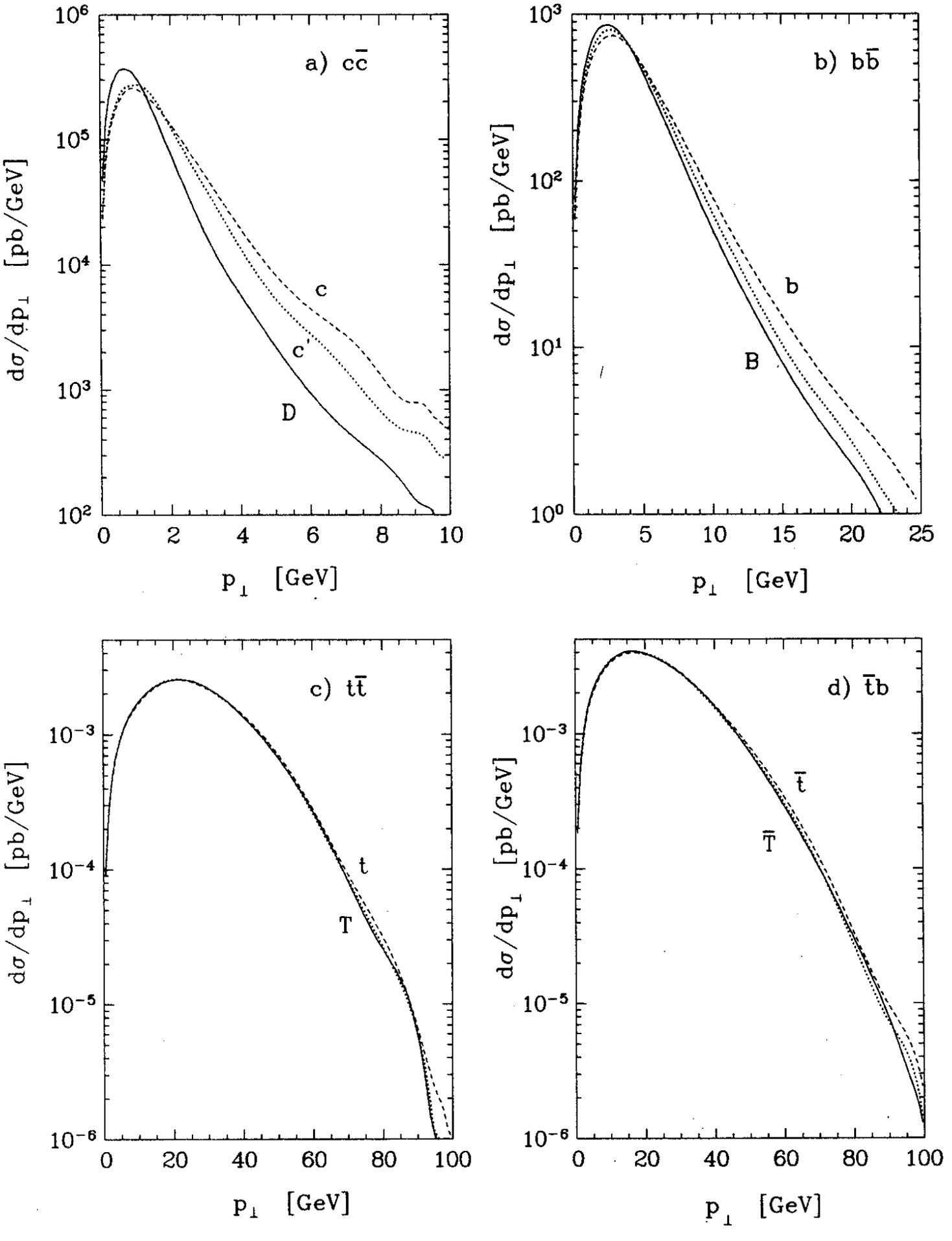
a) $c\bar{c}$
b) $b\bar{b}$
c) $t\bar{t}$
d) $\bar{t}b$
$d\sigma/dp_\perp$ [pb/GeV]
$p_\perp$ [GeV]
c
c'
D
b
B
t
T
$\bar{t}$
$\bar{T}$

Fig. 9

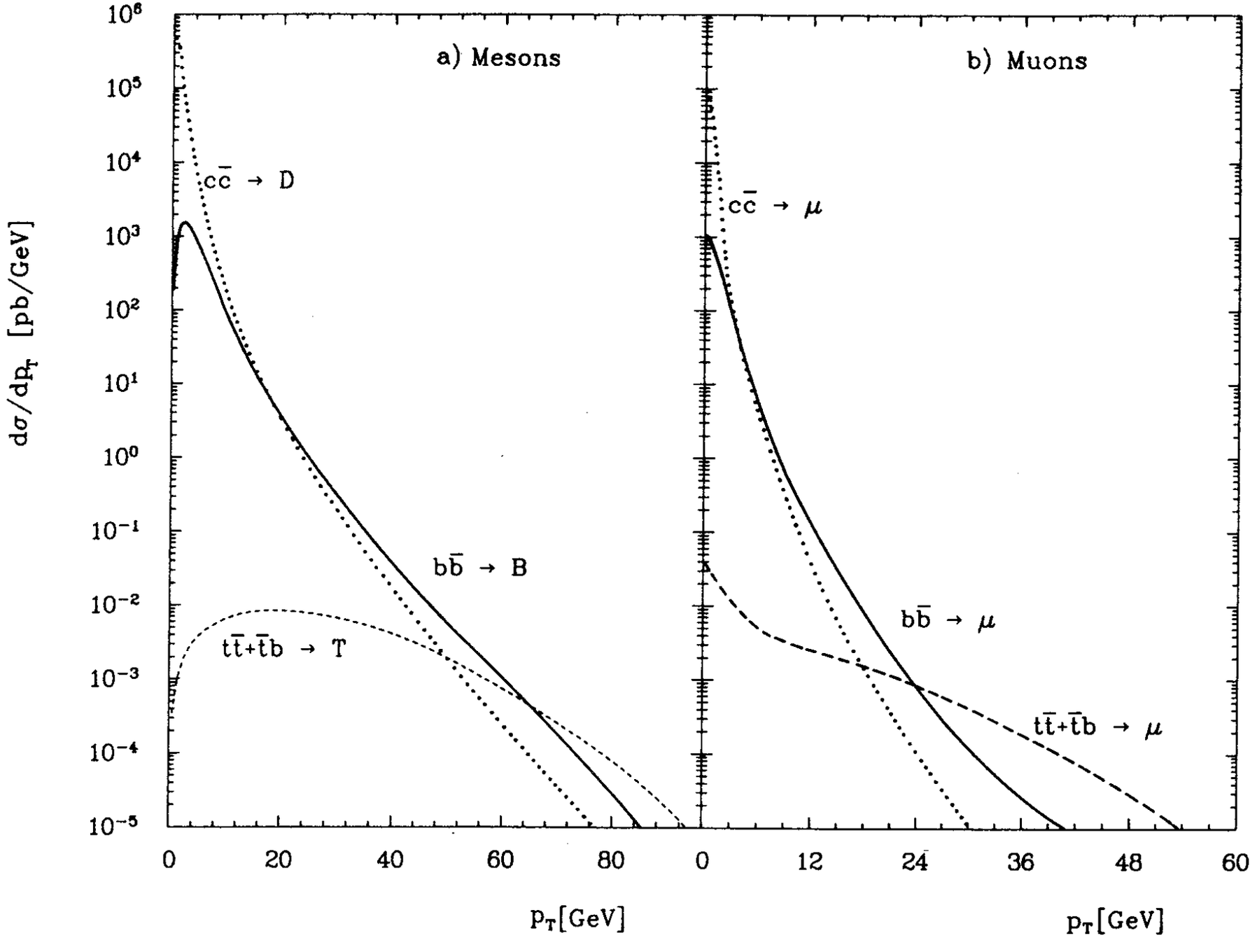
a) Mesons
b) Muons
$c\bar{c} \to D$
$b\bar{b} \to B$
$t\bar{t}+\bar{t}b \to T$
$c\bar{c} \to \mu$
$b\bar{b} \to \mu$
$t\bar{t}+\bar{t}b \to \mu$
$d\sigma/dp_T$ [pb/GeV]
p_T[GeV]
p_T[GeV]
10^6
10^5
10^4
10^3
10^2
10^1
10^0
10^{-1}
10^{-2}
10^{-3}
10^{-4}
10^{-5}
0
20
40
60
80
0
12
24
36
48
60

Fig. 10

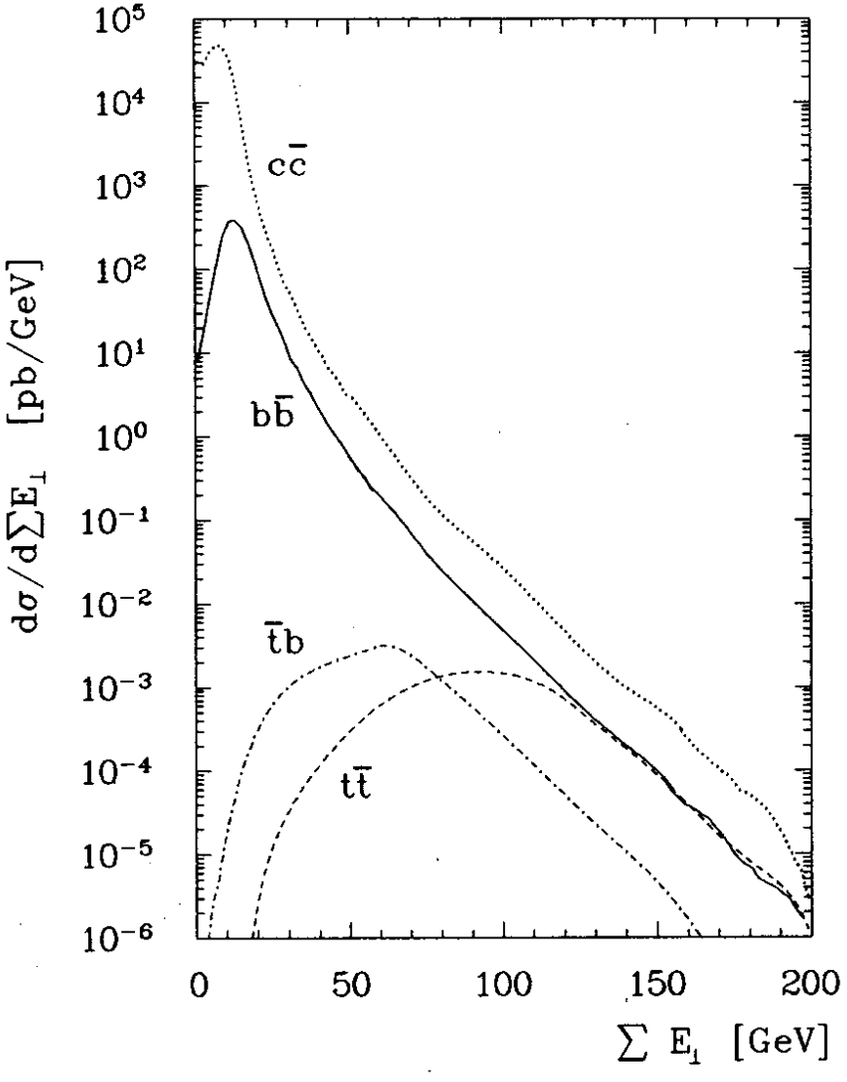
10^5
10^4
10^3
10^2
10^1
10^0
10^{-1}
10^{-2}
10^{-3}
10^{-4}
10^{-5}
10^{-6}
$d\sigma/d\sum E_\perp$ [pb/GeV]
$c\bar{c}$
$b\bar{b}$
$\bar{t}b$
$t\bar{t}$
0
50
100
150
200
$\sum E_\perp$ [GeV]

Fig. 11

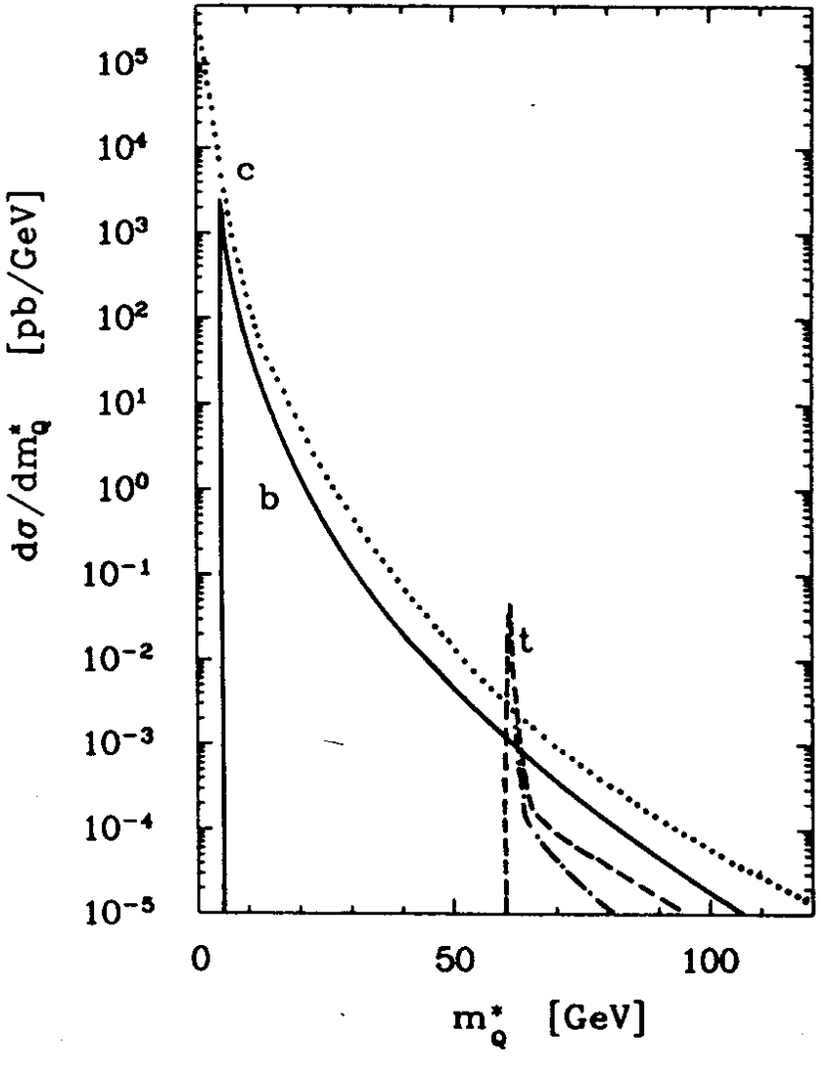
10^5
10^4
10^3
10^2
10^1
10^0
10^{-1}
10^{-2}
10^{-3}
10^{-4}
10^{-5}
$d\sigma/dm_Q^*$ [pb/GeV]
c
b
t
0
50
100
m_Q^* [GeV]

Fig. 12

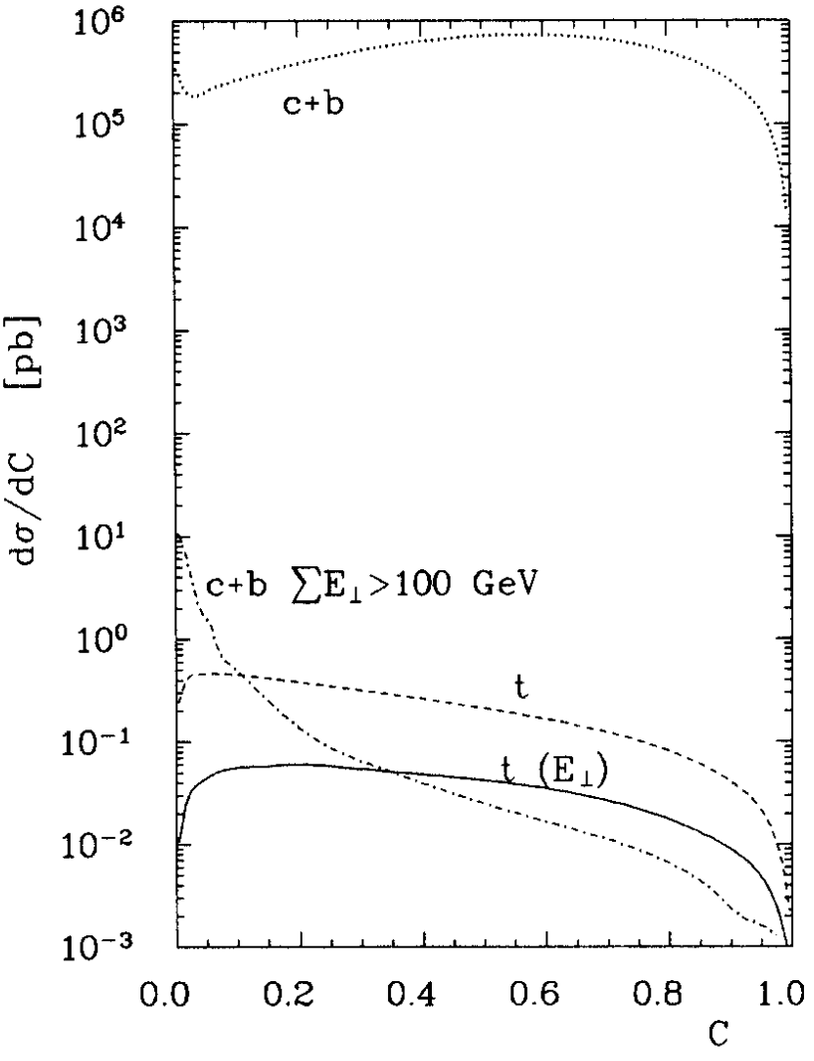
10^6
10^5
10^4
10^3
10^2
10^1
10^0
10^{-1}
10^{-2}
10^{-3}
dσ/dC [pb]
c+b
c+b $\sum E_\perp > 100$ GeV
t
t ($E_\perp$)
0.0
0.2
0.4
0.6
0.8
1.0
C

Fig. 13